

## STACKING SEQUENCE EFFECT ON THE FATIGUE BEHAVIOR OF SINGLE-LAP SHEAR BONDED JOINTS

Francis M.G. Ramírez<sup>1</sup>, Luiz G.M. Lise<sup>2</sup>, Andreas Baumann<sup>1</sup>, Fabian Nowacki<sup>2</sup>,  
Ilona Kunzler<sup>1</sup>, and Joachim Hausmann<sup>1</sup>

<sup>1</sup> Leibniz-Institut für Verbundwerkstoffe GmbH, Kaiserslautern Germany,  
francis.gonzalez-ramirez@ivw.uni-kl.de

<sup>2</sup> ar engineers GmbH, Hamburg, Germany

**Abstract:** The stacking sequence of composite joints, especially the ply orientation at the substrate/adhesive interface, plays an important role in their fracture behavior. However, few works are available on this subject, especially under fatigue loading conditions. This study addresses the stacking sequence effect on the fracture and fatigue behavior of adhesively bonded glass-fiber reinforced polymers. Two layups were considered:  $[0^\circ/90^\circ/90^\circ/0^\circ]_s$  and  $[-45^\circ/90^\circ/45^\circ/0^\circ]_{s2}$ . Single-lap shear (SLS) specimens bonded with a two-component epoxy-based adhesive system (SikaPower<sup>®</sup> 880) were subjected to quasi-static and fatigue testing. Quasi-static tensile tests were executed with the aim of obtaining the load-displacement curves and their respective average fracture ultimate load ( $P_u$ ). Fatigue tests were performed considering a maximum load ( $P_{max}$ ) equal to 40% of  $P_u$ . The evolution of the specimen stiffness ( $E = P/\delta$ ) as a function of the number of cycles (N) was recorded during the SLS fatigue/fracture tests. The fatigue tests considered a sinusoidal waveform with a load ratio ( $R$ ) of 0.1. Fractographic analyses were conducted using a Zeiss Smartzoom 5 digital microscope. The failure mechanisms of both stacking sequences were compared and correlated with the fracture strength, stiffness, and fatigue life results. Both stacking configurations exhibit fiber tear failure under fatigue loading. However, the bidirectional lay-up presented more intra-laminar failure than the quasi-isotropic laminate. The stiffness degradation model used, proved to be accurate to describe the fatigue damage evolution of the SLS, being able to characterize the fatigue life. This information can be used as a guideline in the selection of the best composite joint configuration for high-performance engineering applications.

**Keywords:** Adhesive bonded joints; stacking sequence; fatigue/fracture behavior; single-lap shear specimens.

### INTRODUCTION

The concern for a more sustainable and resource-efficient future in contrast to the rapid consumption of world resources in metals have contributed to great interest in developing and adopting lightweight materials, especially composite materials. Due to their exceptional properties, such as high strength, stiffness-to-weight ratio and durability, fiber-reinforced composites are increasingly used in structural applications, such as aeronautics, automotive, aerospace, and other sectors [1]. An important aspect of an engineering application using composite materials is to evaluate the joint between the components to ensure their performance, structural integrity, and reliability of the overall structure.

Two main joining methods are commonly used to achieve a reliable and strong connection between composite parts: traditional mechanical fasteners (e.g., screws and rivets) and adhesive bonding. The latter offers many interesting advantages compared to the conventional fasteners. In fact, adhesively bonded joints provide lower stress concentrations, the capability of joining dissimilar materials, offer design flexibility and present good damage tolerance [2]. However, such adhesive-bonded parts usually contain micro-cracks and scattered voids introduced during the manufacturing process or the assembly of the joint [3]. Since the presence of such defects can compromise the complete structural integrity [3-4], it is necessary to evaluate the fracture and fatigue behavior, as well as the mechanisms of failure to ensure a safe design of bonded structures.

Although the experimental fatigue campaigns are time-consuming and present high variability in results, it is important to perform these experiments to evaluate the fatigue strength and fatigue life of bonded structures. Such evaluations are of great importance for the fail-safe and damage-tolerance designs of structural components in several industries [5]. The fatigue life of bonded composite joints under tension-tension loading conditions is characterized by different phases. The first one, the nucleation phase, is when micro-discontinuities start to develop. This is followed by the propagation phase, in which the damage propagates up to a critical length, leading to the final phase, the total macroscopic failure [6-8].

To describe the bonded joint fatigue life, different approaches have been developed considering the fatigue damage evolution. According to Degrieck et al. [9], these approaches can be classified into three major categories: models on fatigue life, stiffness degradation or residual strength. The first is based on Stress-Life (S-N) curves, and the other two approaches use macroscopic measurable properties to describe the gradual degradation of the specimen, being established as phenomenological models. The use of stiffness as the damage metric has some advantages as it shows a higher sensitivity to damage progression, has less dispersion in comparison to the residual strength approaches and can be measured using non-destructive methods [10-11]. Some studies used stiffness degradation as a damage parameter to describe the fatigue damage of composite materials and the authors found that the proposed damage function can model the experimental data very well [12-14]. Moreover, a study performed by Zhang et al. [15] showed that the non-linear behavior of Single-lap shear (SLS) adhesively bonded joint fatigue damage, calculated based on the stiffness degradation, has good agreement with the experimental results.

The arrangement of individual composite layers, or the stacking sequence, has been recognized to affect the mechanism of failure of composite joints [8,16,17]. The study performed by Renton et al. [7] analyzed glass/epoxy Single-Lap Joints (SLJs) with unidirectional ( $0^\circ$ ) and multidirectional [45/0/45/0] specimens. The results showed that under fatigue loading, the unidirectional specimens present a cohesive failure, while in their multidirectional specimens, the crack grew through the  $45^\circ$  ply adjacent to the adhesive layer. Similarly, Johnson et al. [18] analyzed the fatigue performance of carbon/epoxy SLJs with three different layups,  $[0/\pm 45/90]_s/[0/\pm 45/90]_{2s}$ ,  $[\pm 45/0/90]_{2s}/[\pm 45/0/90]_{2s}$ ,  $[90/\pm 45/0]_{2s}/[90/\pm 45/0]_{2s}$ . For 0/0 and 45/45 interfaces, fatigue damage was initiated at the adherend/adhesive interface, while for the 90/90 interfaces damage appeared due to ply cracking at the  $90^\circ$  ply. In the case of the 0/0 interface, fatigue damage continues growing at the interface. On the other hand, specimens with 45/45 and 90/90 interfaces presented a mixed mechanism of failure. Regarding fatigue strength, there is no common agreement on the most beneficial layup sequence [8,16,17,19]. According to some studies, such as Meneghetti et al. [8], which compared the fatigue behavior of SLJ with layups of  $[45/0_2]_s$  and  $[45_2/0]_s$ , the presence of a  $45^\circ$  ply at the interface slightly improves the fatigue strength when compared with previous results from  $[0]_6$  joints. Nevertheless, other studies provide contradictory indications, such as Ferreira et al. [19], in which they concluded that a  $0^\circ$  layer on each side of the laminate tends to increase the bending stiffness, improving, in consequence, the fatigue strength.

In this work, the evaluation of the stacking sequence effect on the fracture and fatigue behavior of glass-fiber reinforced polymer bonded joints using SLS specimens is carried out. In addition to providing experimental data for composite joints considering different layups, the failure mechanisms of both

stacking sequences were compared and correlated with the results of stiffness degradation and fatigue damage. These important insights into the fracture mechanisms under fatigue loading can be used as a guideline in the selection of the best composite joint configuration for high-performance engineering applications.

## EXPERIMENTAL PROCEDURES

### Material Properties

The adherends for the SLS specimens were manufactured from multiaxial, non-crimp E-glass fiber fabrics (*Saertex* B-E-840 g/m<sup>2</sup> and Q-E-820 g/m<sup>2</sup>) with 50% fiber volume content and an epoxy resin system (Gurit *PRIME*<sup>TM</sup> 27 and *PRIME*<sup>TM</sup> 37). The two lay-ups are designated as B series and Q series, respectively. To increase the adhesion between the adhesive layer and the adherends, peel-ply fabrics were placed before curing at the bonding surfaces of the plates. The laminates were fabricated using the vacuum-assisted resin infusion (VARI) technique. The specimens were made by bonding two adherends with a two-component epoxy-based adhesive system *SikaPower*<sup>®</sup> 880. Table 1 shows the properties of the adherends, in which the mechanical properties of the Glass Fiber-Reinforced Plastic (GFRP) laminates have been estimated via classical laminate theory and micromechanical formulae.

Table 1: Properties of the laminates used for the SLS specimens.

<i>Laminate</i>	<i>B-E-840g/m<sup>2</sup> (B series)</i>	<i>Q-E-820g/m<sup>2</sup> (Q series)</i>
Layup sequence	[0°/90°/90°/0°] <sub>s</sub>	[-45°/90°/45°/0°] <sub>s2</sub>
E-Modulus (E <sub>x</sub> )	25890 MPa	18900 MPa

The mechanical properties of the adhesive were obtained from the supplier's datasheet [20], as shown in Table 2.

Table 2: Properties of *SikaPower*<sup>®</sup> 880.

<i>Properties</i>	<i>Value</i>
Density	1.2 g/cm <sup>3</sup>
E-Modulus	2100 MPa
Tensile Strength	22 MPa
Elongation at break	3%

### Fabrication of the bonded joints

The GFRP laminates were cut into smaller plates of 130x100 mm<sup>2</sup> using a *Qcut 400 A* automatic wet abrasive cut-off machine with a diamond disk (Figure 1.a). Two steel bands of 0.2 mm were placed on the edges to guarantee the desired adhesive thickness (Figure 1.c). Holes were drilled on the plates and the steel bands to tighten screws ensuring a constant bond line. Masking tape was used to delimit the overlap area while bonding. The adhesive was mixed on a high Speed-Mixer *DAC 150 FV* to fully combine the system and extract any trapped air bubbles (Figure 1.b). Then, just before pouring the adhesive, the overlap area was cleaned with acetone using cotton tissues. The adhesive was poured in a single thick line in the middle of the overlap area and pressed with the other plate (Figure 1.c). This process avoids adding air bubbles during the adhesive application and pushes any remaining dust particles from the center to outside the bonding area. Finally, the screws were tightened, and the excess of adhesive was removed. The joints were cured at 85° C for two hours. Once cured, the plates were cut into their final dimensions using the same cut-off machine (Figure 2). Three specimens resulted from each plate. To guarantee the alignment of the load during testing, two GFRP tabs were pasted on each specimen arm (Figure 2).



Figure 1. Fabrication process of the SLS joints: a) cutting of the plates, b) mixing of the adhesive system and c) bonding process.

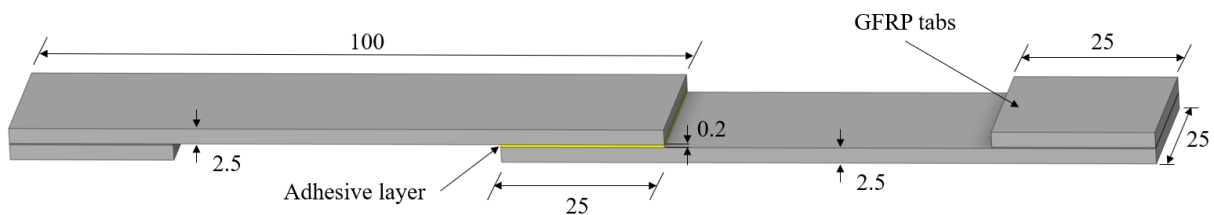


Figure 2. Schematic representation of a Single-Lap Shear specimen (dimensions in mm).

### Fracture and Fatigue tests

In this work, the fracture and fatigue experimental behavior of two different layup configurations was analyzed and compared. In the first place, fracture tests were conducted to attain the average ultimate tensile load ( $P_{u(av)}$ ) of SLS joints. Then, for each configuration, fatigue tests were performed considering a tensile-tensile sinusoidal wave. All the specimens were tested at ambient laboratory environmental conditions, 23°C and 50% of relative humidity.

Three specimens per stacking sequence were submitted to quasi-static tensile loading until failure. The tests were carried out on a Zwick Testing machine coupled with a 10kN loading cell. Fracture tests were performed under displacement control at a rate of 2 mm/min. Once the quasi-static tests were finished and the average ultimate tensile loads were determined, it was possible to establish the fatigue tests' load range of each configuration. A maximum cyclic load equal to 40% of the  $P_{u(av)}$  was settled and a maximum-to-minimum loading ratio  $R = P_{min}/P_{max} = 0.1$  was considered. Fatigue tests were carried out on a MTS servo-hydraulic testing machine. The tests were conducted under load control at a 7 Hz frequency. Three specimens of each configuration were fatigued until failure.

Once the test campaigns were completed, the fracture surfaces were visually observed to have a general overview of the fracture process. Afterwards, to gain a better understanding of their failure mechanisms, some specimens were selected to be studied by microscopy. Furthermore, microsections should verify that stiffness degradation is mainly caused by the bonded area and not the substrate laminates. Usually, a good correlation between the number of transverse cracks and stiffness degradation is possible [21].

### Fractographic analysis

Fractographic analyses were conducted using a Zeiss Smartzoom 5 system. These analyses were performed to correlate the results of the two stacking configurations with the mechanism of failure of some specimens.

## FATIGUE DAMAGE MODEL

To describe the fatigue damage of the SLS specimens, a phenomenological approach based on a stiffness degradation damage parameter was employed. This model is a function of the stiffness evolution of a structural component under fatigue loading. To obtain a quantitative assessment of fatigue damage using stiffness degradation, the approach developed by Mao et al. [13] was used as follows:

$$D(N) = \frac{E_0 - E(N)}{E_0 - E_f} \quad (1)$$

where  $D$  is the accumulated fatigue damage ranging between 0 (initial undamaged state) and 1 (total failure state),  $E_0$  is the initial stiffness,  $E(N)$  is the stiffness after  $N$ th number of cyclic loading of the damaged structure and is the stiffness just before total failure of the specimen.

Based on the study performed by Zhang et al. [15], one can conclude considering the experimental evaluation, that the fatigue damage for a SLS specimen has a non-linear behavior, in which the stiffness degradation is more pronounced at the beginning and close to total failure. Additionally, the study carried out by Lise [14] showed that the fatigue damage evolution for short fiber reinforced thermoplastic materials has a very similar non-linear behavior, divided into three steps: the first shows a high stiffness degradation, followed by a relative constant damage rate and in the third step, a high damage rate leading to the complete failure. Therefore, for the evaluation of the fatigue damage evolution i.e., fatigue damage over the cycles, of the B series and Q series SLS specimens, the following equation was employed [14]:

$$D(N) = 1 - \left(1 - \left(\frac{N}{N_f}\right)^\alpha\right)^\beta \quad (2)$$

where  $\alpha$  and  $\beta$  are the shape parameters,  $N$  is the number of fatigue cycles and  $N_f$  is the number of cycles to failure.

## RESULTS

### Fracture Results

To compare the quasi-static strength between the two SLS stacking configurations, load-displacement curves were generated (Figure 3). In both cases, the curves were consistent; the load increased linearly and after reaching  $P_u$ , it dropped drastically by a sudden failure. Clearly, the maximum peak load was achieved by the Q series. The average ultimate load of the Q series was 7298.2 N, while the  $P_{u(av)}$  of the B series was 22.7% less (5640.3 N) resulting in an apparent shear strength of 11.67 MPa and 9.02 MPa, respectively. For both layup sequences, the stiffness was approximately the same (Table 1). As can be seen in Figure 4, the B series exhibited a fiber tear failure (FT) in the whole overlap area, while the Q series presented a mixed mechanism of failure [22].

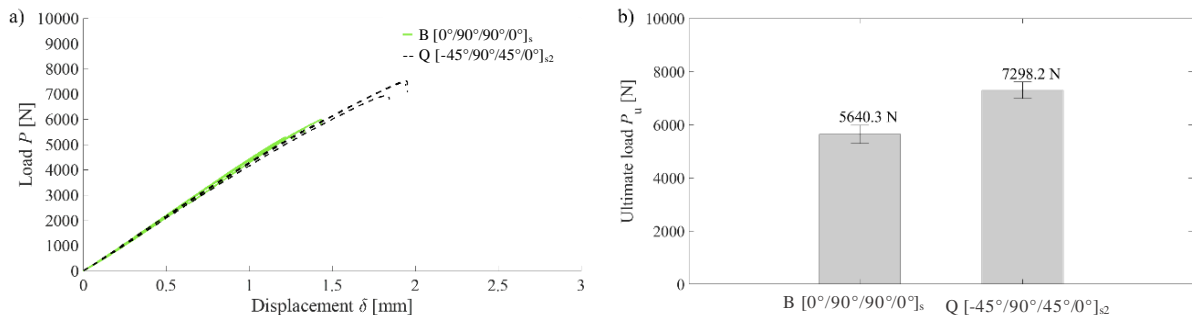


Figure 3. (a) Load-displacement curves and (b) average ultimate loads with standard deviation.

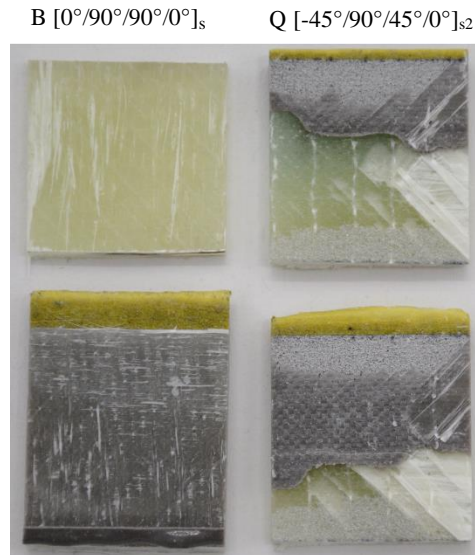


Figure 4. Fracture surface of the SLS specimens under quasi-static loading.

### Fatigue Damage Results

The experimental fatigue life results obtained from constant amplitude tension-tension fatigue tests are shown in Table 3. As one can see, the Q series showed a significantly longer fatigue life in comparison to the B series.

Table 3: Fatigue life at  $P_{\max} = 0.4 P_u$  for both layup sequences.

<i>Fatigue life</i>	<i>B series</i>	<i>Q series</i>
Number of cycles to failure	17279	80567
Standard deviation	4.24%	13.69%

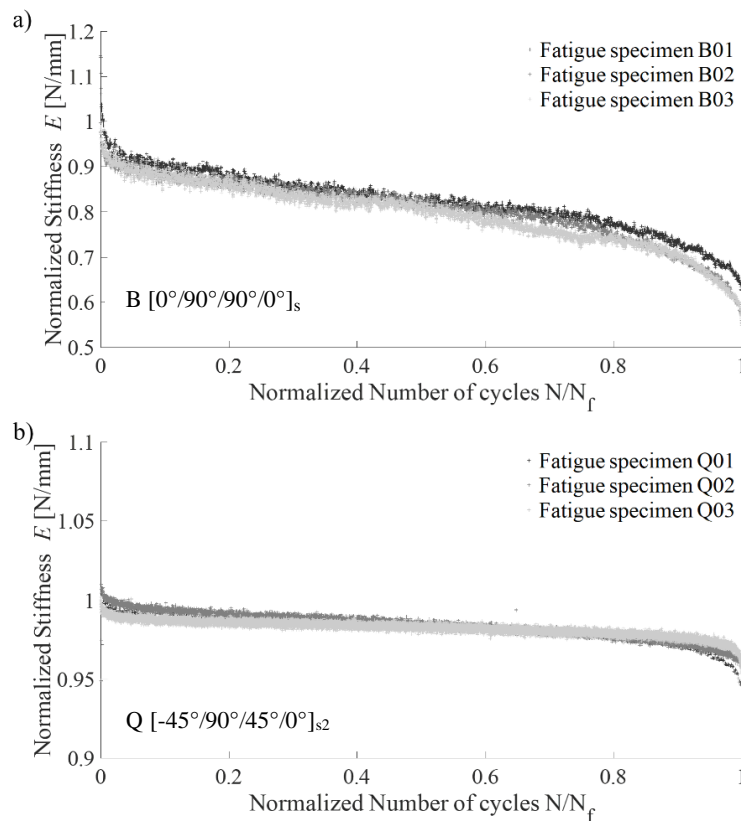


Figure 5. Stiffness degradation of the SLS specimens under fatigue loading: a) B series, b) Q series.

For the calculation of the fatigue damage parameter, the stiffness was measured at equal intervals during cyclic loading. The stiffness degradation behavior (Figure 5) agrees with the results reported by Zhang [15] for SLS specimens, where a higher degradation is observed in the first and last stages. It can be observed that for the B series, the stiffness degraded by around 40%, compared to less than 5% for the Q series.

The results obtained for the stiffness along the fatigue cycles were applied to Eqn. (1) and the fatigue damage evolution was calculated based on the normalized fatigue life (Figure 6). The damage evolution for the B and Q series showed three stages. The first is characterized by a rapid initial stiffness degradation, causing the damage to increase rapidly, followed by the second stage, where the damage increases steadily with a gradual reduction of stiffness. In the third stage, a severe accumulation of damage causes a sudden degradation of stiffness, leading to total failure of the SLS specimens.

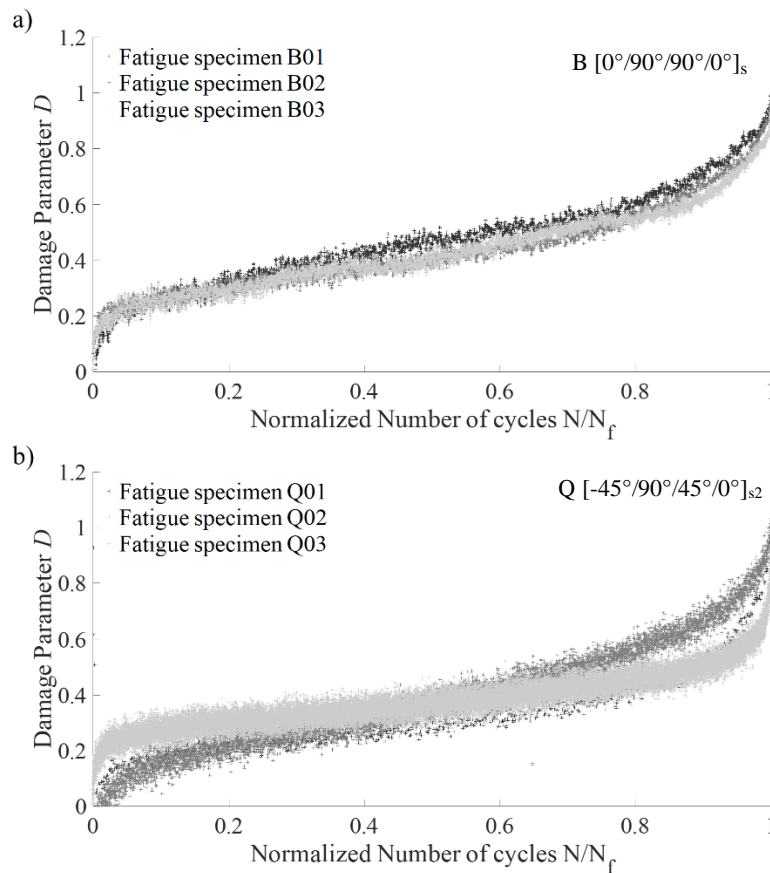


Figure 6. Damage parameter evolution of the SLS specimens under fatigue loading: a) B series, b) Q series.

Once the fatigue damage was evaluated, the Eqn. (2) was applied to the experimental results to define the shape parameters. Therefore, for each layup sequence, the model parameters were determined using a non-linear least-squares curve fitting analysis. The shape parameter values of  $\alpha$  and  $\beta$  and the coefficient of determination ( $R^2$ ) are listed in Table 4.

Table 4: Model parameters for both layup sequences.

Parameter	<i>B-E-840g/m<sup>2</sup> (B series)</i>	<i>Q-E-820g/m<sup>2</sup> (Q series)</i>
$\alpha$	0.185	0.473
$\beta$	0.259	0.362
$R^2$	0.963	0.974

Based on the  $R^2$  values, Eqn. (2) proved to be effective in modelling the fatigue damage behavior, presenting a high accuracy between the predicted and experimental results. Considering the values obtained for the shape parameters, the damage evolution rate ( $DR$ ) was evaluated by the derivative of Eqn. (2), as shown in Figure 7. During the first stage, the B series exhibited a higher accumulated damage rate than in comparison to the Q series. Regarding the second stage, in which the damage increases steadily and slowly, the Q series showed a slightly greater damage rate than the B series. In the third stage, the B series showed a higher damage rate, reaching more rapidly the total failure than the Q series.

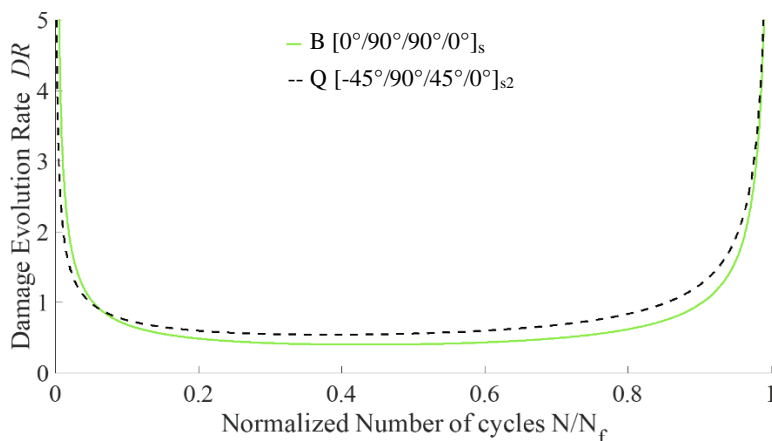


Figure 7. Damage evolution rate of the SLS specimens under fatigue loading.

For fatigue loading, the fracture surfaces of both stacking sequences exhibit fiber tear failure (Figure 8). Clearly, it can be observed that there was an extensive delamination migration between the plies and fiber breakage. Fatigue loads can lead to gradual changes in the material, such as local reductions in stiffness and the development of local microcracking. In fact, plies that are at an angle with respect to the driving force are more prompt to matrix cracking, which in time can lead to delamination within the thickness [23].

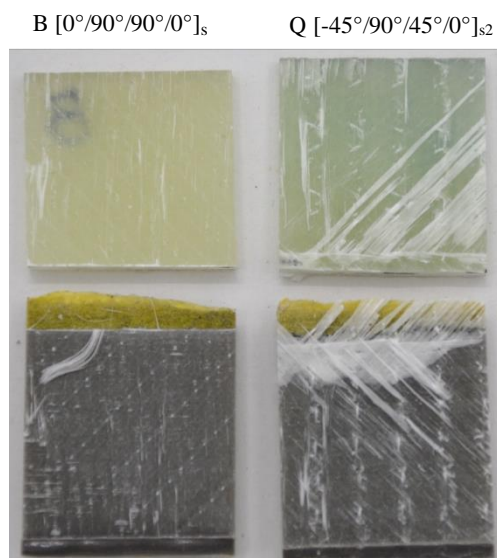


Figure 8. Fracture surface of the SLS specimens under fatigue loading.

#### Fractography and microsectioning analyses

By high magnification images, it becomes evident that for B series inter- and intralaminar failure was the predominant failure mode for both quasi-static loading as well as fatigue loading (Figure 9). Fiber

tear failure in the substrate is inter-laminar in nature because all fracture surfaces show fibers in 0° and 90°. Only inter-laminar failure is likely to show by both fiber reinforcements.

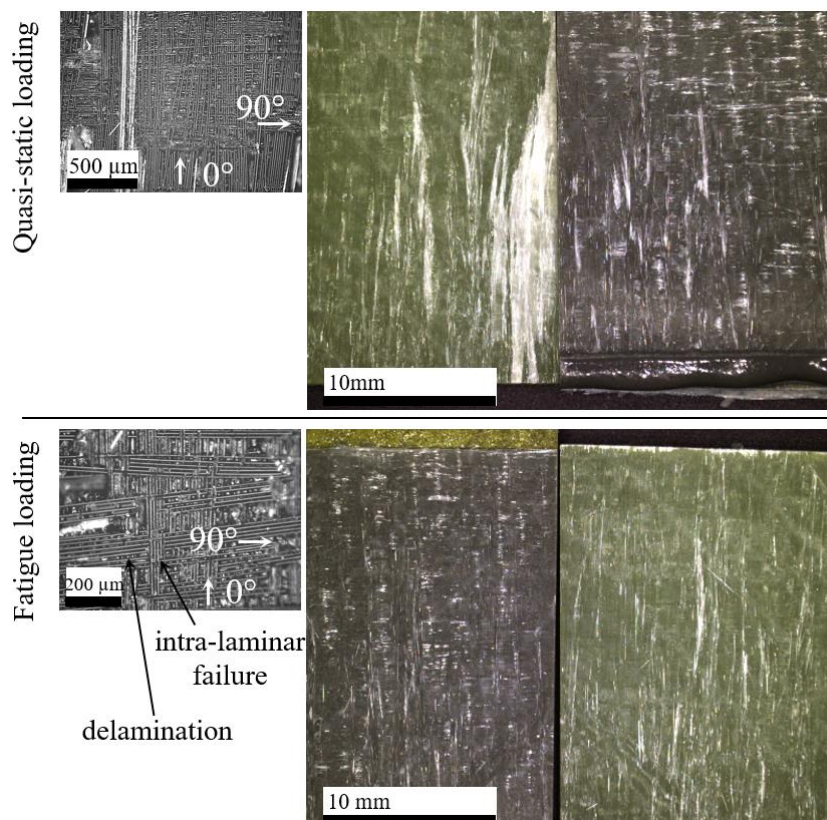


Figure 9. Fracture surface of the SLS specimens B  $[0^\circ/90^\circ/90^\circ/0^\circ]_s$ .

In contrast to stacking sequence B, the Q series shows an altered fracture surface because of cyclic loading. For quasi-static loading, a mixed-failure mode can be seen (Figure 10) ranging from cohesive failure (C), over adhesive failure (A) to fiber tear failure (FT). The fracture surface is symmetric with respect to the overlap length and transitions from one substrate to the other nearly midway. Moreover, the cracking changes from this mixed behavior to pure substrate failure. From the visible 45° layer it is likely also interlaminar failure. Some small pores in the adhesive are visible near the edge of the overlap, which leads to cohesive failure of the adhesive in this region under monotonic loading.

From the fracture surfaces it is evident that during fatigue especially the interfaces between adjacent layers with different stacking sequences are prone to cracking. One possible explanation could be that different Poisson's ratios in combination with peel stresses promote delamination. This would be in accordance with edge effects often observed in fatigue of multiaxial laminates. In the case of the Q series, the crack path delaminates mainly through the 45° ply adjacent to the adhesive layer, while in the B series fracture surface exhibited delamination and a high degree of intra-laminar failure between the 0° and 90° plies adjacent to the interface.

In addition to the analysis of the fracture surface itself, microsections are prepared outside the overlap length with a special focus on the transversely loaded plies. Transverse cracks are usually the first damage to occur in multidirectional laminates and initiate most other major damage types like delamination and fiber fracture. The absence of transverse matrix cracks in all investigated specimens shows that stiffness degradation is mainly concentrated in the bond area but not in the laminate of the adherends. Matrix cracks were neither observed in a fatigue-loaded sample nor in those fractured quasi-statically. Additionally, the microsections also revealed a minor number of pores. An aerial evaluation leads to 1.7% and 0.8% of pores for the B and Q series respectively. From the fracture surfaces this seems to affect the sample performance only slightly. Further research is still necessary in this context.

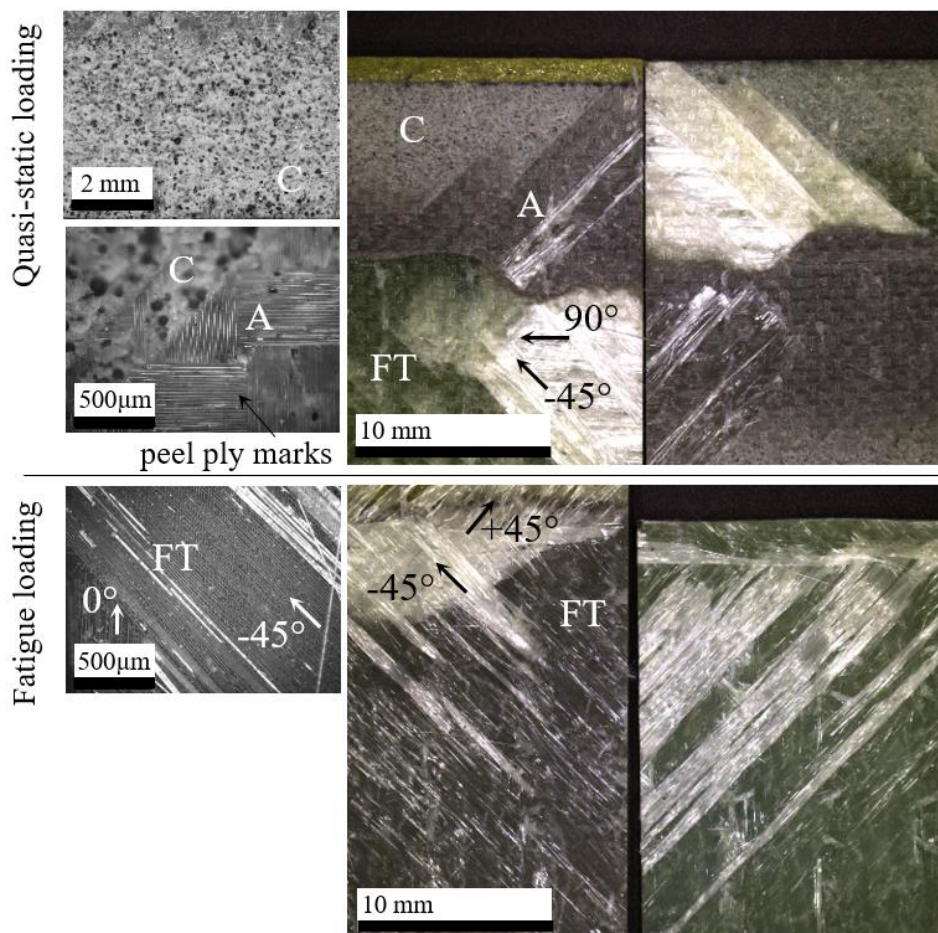


Figure 10. Fracture surface of the SLS specimens Q  $[-45^\circ/90^\circ/45^\circ/0^\circ]_{s2}$ .

## CONCLUSION

The behavior of adhesively bonded GFRP single-lap composite joints under static and fatigue tensile loading was experimentally investigated. Two different stacking sequences were evaluated and compared: B  $[0^\circ/90^\circ/90^\circ/0^\circ]_s$  and Q  $[-45^\circ/90^\circ/45^\circ/0^\circ]_{s2}$ . The fatigue damage evolution was analyzed based on a phenomenological stiffness degradation model. Afterwards, a microscopic study was conducted to understand the effect of the stacking sequences on the mechanism of failure of the joints. The quasi-static results showed a higher fracture strength for the stacking sequence with a  $45^\circ$  layer at the interface. This improvement of 23% in the ultimate strength can be due to the complex fracture path of this configuration.

The stiffness degradation model used in this work proved to be accurate for describing the fatigue damage accumulation on single-lap joints. Additionally, a power law precisely described the fatigue damage evolution of single-laps bonded joints. For both stacking sequences the square error ( $R^2$ ) was lower than 4%. In both stacking sequences, a higher stiffness degradation was observed at the damage initiation phase and final fatigue stage just before total failure. The B series presented a high stiffness degradation of 40%, while in the case of the Q series, the stiffness only decreased by 5%. Moreover, the B series exhibit a slightly higher damage evolution rate in the damage initiation phase. This trend has been also found in other works [16]. It has been observed that  $0^\circ$  layers are usually the locus of intra-laminar delamination, which could accelerate failure. For fatigue loading, both stacking configurations exhibit fiber tear failure. However, the B series presented more intra-laminar failure than the Q series. For this reason, the B series fatigue life was significantly lower than the Q series. It is important to highlight the fact that the maximum force ( $P_{max}$ ) was higher for the Q series.

## ACKNOWLEDGEMENTS

We acknowledge the support from Prof. Paul Geiß from the Workgroup Materials and Surface Technologies of RPTU Kaiserslautern-Landau in specimen manufacturing.

The project “FANTeStick – Fatigue Analysis and Test Procedures for the Design of Bonded Joints” is funded by the Federal Ministry for Economic Affairs and Climate Action on the basis of a decision by the German Bundestag (funding reference KK5003702EB0).

## REFERENCES

- [1] R. Fragoudakis and A. Saigal. (2011), “Predicting damage accumulation in glass fiber reinforced plastics through cumulative damage models,” *ICCM International Conferences on Composite Materials*.
- [2] I. Ashcroft, J. P. Casas-Rodriguez, and V. Silberschmidt. (2008), “Mixed-mode crack growth in bonded composite joints under standard and impact-fatigue loading,” *J Mater Sci*, vol. 43, pp. 6704–6713.
- [3] Y. Kouno, M. Imanaka, R. Hino, M. Omiya, and F. Yoshida. (2020), “R-curve behavior of adhesively bonded composite joints with highly toughened epoxy adhesive under mixed mode conditions,” *Int J Adhes Adhes*, vol. 105, p. 102762.
- [4] F. M. G. Ramírez, M. F. S. F. de Moura, R. D. F. Moreira, and F. G. A. Silva. (2021), “Experimental and numerical mixed-mode I + II fracture characterization of carbon fibre reinforced polymer laminates using a novel strategy,” *Compos Struct*, vol. 263.
- [5] M. M. Abdel Wahab. (2012), “Fatigue in Adhesively Bonded Joints: A Review,” *ISRN Materials Science*, vol. 2012, pp. 1–25.
- [6] G. Meneghetti, M. Quaresimin, and M. Ricotta. (2012), “Damage mechanisms in composite bonded joints under fatigue loading,” *Compos B Eng*, vol. 43, no. 2, pp. 210–220.
- [7] W. J. Renton and J. R. Vinson. (1975), “Fatigue Behavior of Bonded Joints in Composite Material Structures,” *J Aircr*, vol. 12, no. 5, pp. 442–447.
- [8] G. Meneghetti, M. Quaresimin, and M. Ricotta. (2010), “Influence of the interface ply orientation on the fatigue behaviour of bonded joints in composite materials,” *Int J Fatigue*, vol. 32, no. 1, pp. 82–93.
- [9] J. Degrieck and W. Van Paeppegem. (2001), “Fatigue damage modeling of fibre-reinforced composite materials: Review,” *Appl Mech Rev*, vol. 54, no. 4, pp. 279–300.
- [10] A. L. Highsmith, K. L. Reifsnider. (1982), A. International, and A. S. for T. and Materials, *Stiffness-Reduction Mechanisms in Composite Laminates*. ASTM International.
- [11] R. Talreja. (1987), *Fatigue of Composite Materials*. in A Technomic Publishing Company book. Taylor & Francis.
- [12] P. Ladeveze and E. LeDantec. (1992), “Damage modelling of the elementary ply for laminated composites,” *Compos Sci Technol*, vol. 43, no. 3, pp. 257–267.
- [13] H. Mao and S. Mahadevan. (2002), “Fatigue damage modelling of composite materials,” *Compos Struct*, vol. 58, no. 4, pp. 405–410.
- [14] L. G. M. Lise. (2020), “Investigation of damage evolution due to cyclic mechanical loads and load/frequency spectra-effects in short-fibre-reinforced thermoplastics,” Universidade Federal de Santa Catarina, Florianópolis.
- [15] Y. Zhang, A. P. Vassilopoulos, and T. Keller. (2008), “Stiffness degradation and fatigue life prediction of adhesively-bonded joints for fiber-reinforced polymer composites,” *Int J Fatigue*, vol. 30, no. 10–11, pp. 1813–1820.
- [16] S. Purimpat, R. Jérôme, and A. Shahram. (2013), “Effect of fiber angle orientation on a laminated composite single-lap adhesive joint,” *Advanced Composite Materials*, vol. 22, no. 3, pp. 139–149.
- [17] J. Kupski, S. Teixeira de Freitas, D. Zarouchas, P. P. Camanho, and R. Benedictus. (2019), “Composite layup effect on the failure mechanism of single lap bonded joints,” *Compos Struct*, vol. 217, pp. 14–26.

- [18] W. S. Johnson. (1985), *Influence of interface ply orientation on fatigue damage of adhesively bonded composite joints [microform]* / W. S. Johnson and S. Mall. in NASA technical memorandum; 86443. Hampton, Va: National Aeronautics and Space Administration, Langley Research Center.
- [19] J. A. M. Ferreira, P. N. Reis, J. D. M. Costa, and M. O. W. Richardson. (2000), “Fatigue behaviour of composite adhesive lap joints,” 2000.
- [20] Sika. (2022), “Datasheet: SikaPower®-880.”
- [21] X. Li, J. Kupski, S. Teixeira De Freitas, R. Benedictus, and D. Zarouchas. (2020), “Unfolding the early fatigue damage process for CFRP cross-ply laminates,” *Int J Fatigue*, vol. 140.
- [22] ASTM D5573–99. (2019), “Standard Practice for Classifying Failure Modes in Fiber-Reinforced-Plastic (FRP) Joints”.
- [23] Srinivasan. Sridharan. (2008), *Delamination behaviour of composites*. Woodhead Pub.